

# Effects of non-ideal biased grids on drifting particle distribution functions

by  
Jeffrey Klenzing

A research proposal submitted to  
the faculty of the University of  
Texas at Dallas in partial  
fulfillment of the requirements  
for the degree of Doctor of  
Philosophy

September 2006

# Contents

<b>1</b>	<b>Introduction</b>	<b>1</b>
1.1	A Brief Overview . . . . .	1
1.2	Measurement of a Drifting Particle Distribution . . . . .	2
1.3	The Ram Wind Sensor . . . . .	5
<b>2</b>	<b>Analysis Techniques</b>	<b>7</b>
2.1	The Knudsen Analysis Technique . . . . .	7
2.2	Non-Uniform Potential . . . . .	10
2.3	Angular Considerations . . . . .	10
2.4	Need for an Improved Technique . . . . .	11
<b>3</b>	<b>Discrete Analysis</b>	<b>13</b>
3.1	A Simple Construct . . . . .	13
3.2	The Idealized Solution . . . . .	15
3.3	Perturbation Considerations . . . . .	16
3.4	The General Solution . . . . .	17
3.5	A Proposed Solution . . . . .	18

3.6	Data Fitting . . . . .	20
<b>4</b>	<b>Methodology</b>	<b>21</b>
4.1	A Brief Description of ANSYS . . . . .	21
4.2	Verification . . . . .	22
4.3	Research Approach and Goals . . . . .	23
4.3.1	The ANSYS Code . . . . .	23
4.3.2	The FORTRAN Simulator . . . . .	26
4.3.3	The Data-Fit Routine . . . . .	26
<b>5</b>	<b>Summary and Conclusions</b>	<b>27</b>

## **Abstract**

The thesis proposal detailed here covers the study of the effects of non-ideal biased grids on drifting particle distribution functions. Instruments such as the Retarding Potential Analyzer measure the distribution of flux as a function of ion energy by use of these biased grids. A similar technique can be used to measure the flux distribution of neutral particles with the Ram Wind Sensor, a new instrument in development. In order to fit collected data to physical parameters, the interaction of charged particles with the biased grid must be studied thoroughly. The program of study outlined in this proposal will discuss several shortcomings of non-ideal biased grids on data analysis techniques. In addition, I propose a new method of data analysis, which will take these shortcomings into account.

# Chapter 1

## Introduction

### 1.1 A Brief Overview

One of the fundamental instruments of space science is the Retarding Potential Analyzer (RPA). RPAs have successfully been flown on satellites since the late 1950's, including Sputnik [11], Atmospheric Explorer [6], Dynamics Explorer [7], and the DMSP family of satellites.

The function of the RPA is to measure the ion flux distribution in the ram direction as a function of energy, as outlined further in Section 1.2. At the heart of the RPA is a set of biased grids through which the particles of interest pass. The interaction between these charged particles and the grids is the focus of the study proposed here.

The retarding grid structure is also fundamental in the construction of a new instrument known as the Ram Wind Sensor (RWS), designed to measure the flux distribution of neutral atoms with constant angle of attack. This will be further outlined in the Section 1.3.

Over the years, various curve-fitting techniques have been developed to extract parameters such as density, temperature, drift velocity, and species composition from RPA data. One of these techniques will be described in Chapter 2, as well as several perturbations not considered in the ideal case.

A new analysis technique designed to consider these perturbations is outlined in Chapter 3. This technique uses a discrete analysis to simulate a set of collected currents as a function of voltage bias on the grid for a given incoming distribution of ions.

Chapter 4 outlines the methodology used to simulate the values of current. In addition, several practical considerations will be discussed in using this equation in a curve-fitting routine.

## 1.2 Measurement of a Drifting Particle Distribution

The RPA measurement technique consists of collecting ions above a specified energy while excluding lower energy ions. This is achieved by passing the ions through a series of biased grids prior to measuring the ion current. Figure 1 shows a cartoon drawing of a normalized drifting Maxwellian distribution. The temperature has been artificially inflated over that found in a naturally occurring ionosphere such that  $v_{drift} = v_{thermal}$  for the purpose of illustration. Both of these values have been set to a magnitude of 1 for simplicity. The graph is set up such that a negative velocity indicates ions moving toward the collector, and a positive velocity indicates those moving away from it. Note this implies that a certain fraction of ions in the distribution cannot be collected.

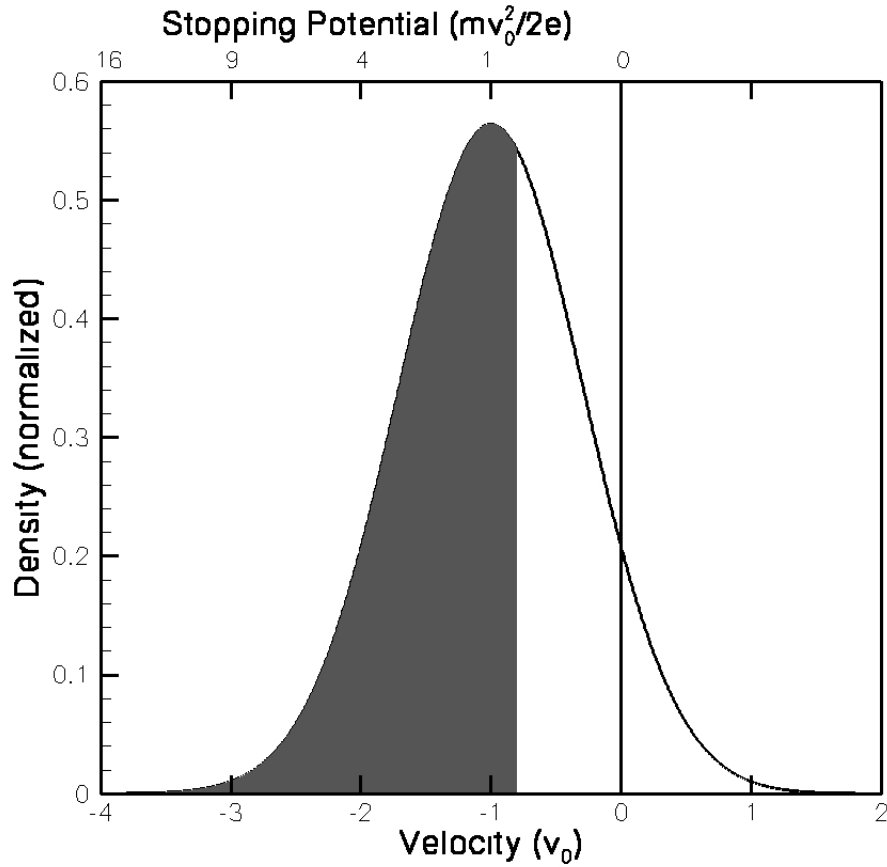


Figure 1: A sample density distribution. The shaded portion of the curve illustrates the ions collected for a particular bias voltage. Ions with a positive velocity relative to the collector are moving away from the collector and cannot be collected.

A specified voltage is applied to one of the grids to select ions above a given energy. This grid is referred to as the RV (retarding voltage) grid. Ions with a kinetic energy less than the stopping energy specified at the RV grid will not pass through the grid to be collected. The shaded portion of Figure 1 represents those ions moving fast enough to penetrate the RV grid for a given applied potential ( $0.32 \frac{mv_0^2}{e}$ ). Note that collected current decreases as stopping potential increases, resulting in a current-voltage (IV) characteristic curve. The IV

curve shown in Figure 2 is derived from the sample distribution shown in Figure 1.

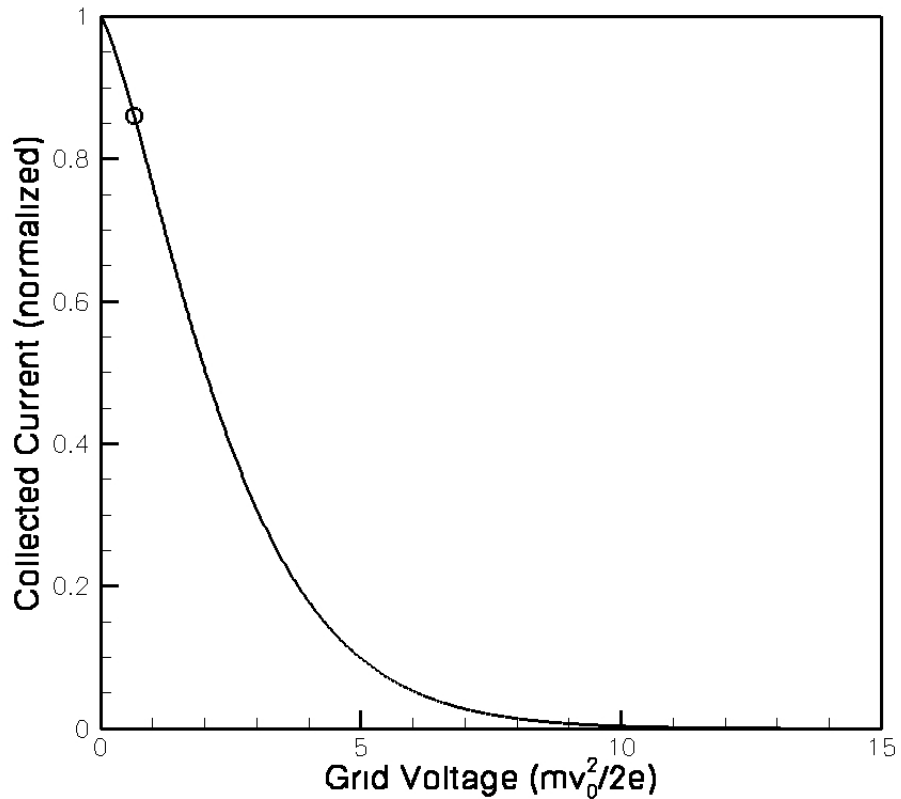


Figure 2: *The IV Curve corresponding to the sample distribution in Figure 1. The circle indicates the current collected for the applied RV in Figure 1.*

By comparing successive current measurements as a function of stopping potential, the relative flux of particles having energies between the specified energy values can be measured.

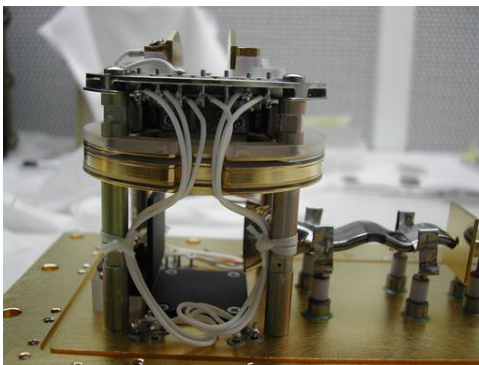
$$\Delta\psi \propto I_{(j)} - I_{(j+1)} \quad (1.1)$$

where  $\psi$  represents the flux and  $I$  is the measured current. If a distribution function is assumed (in this case Maxwellian), then the parameters that uniquely determine the distri-

bution (such as drift velocity, temperature, and particle mass) can be obtained by fitting IV curves like that in Figure 2. This process will be described in further detail in Chapter 2.

### 1.3 The Ram Wind Sensor

An exciting new instrument being developed by the University of Texas at Dallas is the Ram Wind Sensor (RWS). The first space flight of this instrument will be on C/NOFS, the Communications/Navigation Outage Forecast System satellite. C/NOFS consists of a low inclination satellite in combination with a system of ground-based computational models. The RWS will be flown along with a cross-track drift sensor. Together, these two sensors [8],[9] will be able to obtain the three-dimensional neutral wind velocity vector. The RWS determines the ram component of the wind by measuring the flux distribution in the ram direction. Figure 3a shows the interior of the engineering model of the RWS. Figure 3b shows the completed RWS delivered for integration onto the C/NOFS satellite.



(a) Engineering Model



(b) Flight Model

Figure 3: *Images of the Ram Wind Sensor*

The RWS instrument is mounted on the ram surface of a satellite to mitigate wake effects and to prevent interference to the neutral flow from obstacles such as boom systems. Figure

4 shows the conceptual block diagram of the RWS. The ionospheric particles enter the small knife-edge aperture from the left of the diagram. The beam of particles first flows between two biased plates designed to collect ions and electrons, leaving only the neutral particles in the beam. Critical surfaces of the device are coated with black nickel [1] to suppress photons.

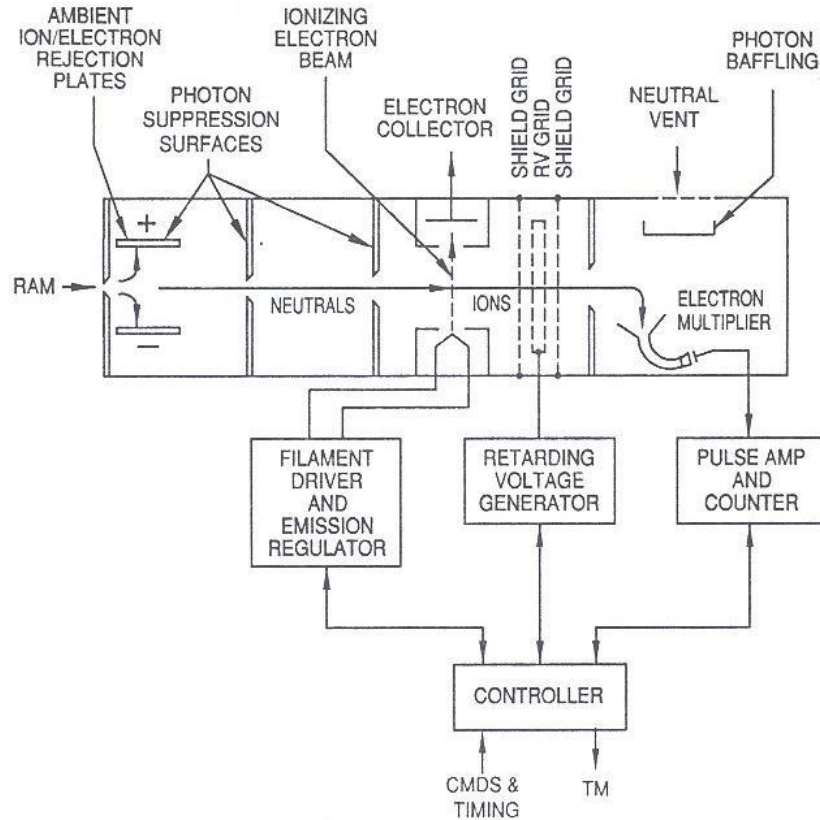


Figure 4: *Conceptual Block Diagram of the RWS*

A cross-track beam of energetic electrons is used to ionize a small fraction of the incoming neutral particles. The distribution of the resulting ions can then be analyzed with an RV grid, as described in the previous section. A channel electron multiplier (CEM) is used to detect the ions after they have passed through the RV grid. The sensitivity of the CEM is such that the small numbers of ionized neutrals at high altitudes can be detected.

# Chapter 2

## Analysis Techniques

### 2.1 The Knudsen Analysis Technique

The 1966 technique for analysis of drifting Maxwellian distributions of ions developed by Knudsen [10] is often used in conjunction with least-squares fitting routines to fit a distribution to a data set. First we consider that each ion species is in a thermal equilibrium subject to a drifting Maxwellian distribution over ram velocity ( $v_{\perp}$ ).

$$n_j(v_{\perp}) = \frac{n_{j0}}{\sqrt{2\pi k_B T/m_j}} \exp\left[-\frac{m_j(v_{\perp} - v_{j0})^2}{2k_B T}\right] \quad (2.1)$$

where  $n_{j0}$  is the total density,  $m_j$  is the ion mass,  $k_B$  is Boltzmann's constant,  $T$  is the ion temperature, and  $v_{j0}$  is the ion drift in the rest frame of the instrument. We can simplify this expression by using a substitution for thermal velocity

$$\alpha_j = \sqrt{\frac{2k_B T}{m_j}} \quad (2.2)$$

so that

$$n_j(v_\perp) = \frac{n_{j0}}{\alpha_j \sqrt{\pi}} \exp \left[ - \left( \frac{v_\perp - v_{j0}}{\alpha_j} \right)^2 \right] \quad (2.3)$$

We assume that all ions below the stopping energy are rejected. This energy value corresponds to a stopping velocity below which no ions will be collected.

$$v_{j-stop} = \sqrt{\frac{2\varepsilon_{stop}}{m_j}} \quad (2.4)$$

We can then eliminate the mass term by substituting  $\alpha_j$ .

$$v_{j-stop} = \alpha_j \sqrt{\frac{2\varepsilon_{stop}}{k_B T}} \quad (2.5)$$

If the potential of the grids is planar and normal to the velocity of the incoming particles and if the grids are considered to have negligible thickness, then the total number of each ion species collected per second will correspond to

$$\mathcal{N}_j = \int_{v_{j-stop}}^{\infty} \chi A v n_j(v) dv \quad (2.6)$$

where  $\chi$  is the total optical transparency of the grid stack and  $A$  is the area of the aperture.

The collected current will be

$$I = e \sum_j \mathcal{N}_j \quad (2.7)$$

where  $e$  is the fundamental charge. We integrate over  $v$  for a given species, yielding

$$\mathcal{N}_j = \chi A \frac{n_j v_{j0}}{2} \left[ 1 + \operatorname{erf}(\kappa_j) + \frac{\exp(-\kappa_j^2)}{\sqrt{\pi} v / \alpha_j} \right] \quad (2.8)$$

where

$$\kappa_j = \frac{v_{j0} - v_{j-stop}}{\alpha_j} \quad (2.9)$$

The total current collected will be

$$I(\varepsilon_{stop}) = e\chi A \sum_j \frac{n_j v_{j0}}{2} \left[ 1 + \text{erf}(\kappa_j) + \frac{\exp(-\kappa_j^2)}{\sqrt{\pi}v/\alpha_j} \right] \quad (2.10)$$

In principle, Equation 2.10 can be used in a least-square or a chi-square fit routine to uniquely determine  $n_j$ ,  $v_{0j}$ , and  $T$ , assuming that all species are at the same temperature. If the drift velocity is the same for all species, then

$$v_{j0} = v_0 \quad (2.11)$$

for all  $j$ , and we only need to fit for  $m + 2$  parameters, where  $m$  represents the number of species under consideration.

In practice, these relatively simple assumptions do not fully describe the particle trajectories. Perturbations on the ideal case may arise from many factors, such as the non-uniformity of the potential due to the grid structure, the arrival angle of incoming ions, contaminants on the grid surface, and space charge effects. The work proposed here concentrates on the first two perturbation sources, since these effects are likely to dominate in many spacecraft scenarios.

## 2.2 Non-Uniform Potential

The geometry of a meshed grid system will set up a non-uniform potential in the grid plane, as described by Hanson *et al.* [6], with the applied potential appearing near the grid wires and a lower potential in the center of each hole. This allows some ions with energy just below the stopping energy (referred to hereafter as threshold ions) to pass through the grid depending on their relative position and trajectory with respect to the grid wires. This has the effect of increasing the collected current above that predicted by the formula above (Equation 2.10).

In practice, the leakage of ions can be reduced by using a double-grid system to reduce the lowest potential seen in the grid plane. A triple-grid system was recently proposed as a measure to further reduce leakage [4]. Further studies by Chao [2], [3] suggest using an depressed retarding potential in fitting calculations, based on the average potential in the RV grid plane.

While recent simulation work has been done with flat grid systems, in practice these grids are often woven, producing further perturbations in the grid-plane potential.

## 2.3 Angular Considerations

While it does reduce the total leakage, the double-grid system provides another distortion in the collected current. The previous calculations neglect the effects of any transverse velocity components that the incoming ions may have. These velocities may result from a thermal distribution as well as from a net drift of the ions parallel to the plane of the grid.

Figure 5 illustrates this problem in cartoon form. Depending on the relative grid orientations, a portion of the threshold ions may be deflected due to the angular trajectory, thus reducing the expected leakage. Ions may be either deflected by the second grid (Figure 5c) or translated along the grid plane (Figure 5d). Near the edge of the instrument, particles may be translated far enough away to miss the collector. Either of these effects will change the total leakage of the system, and therefore change the IV characteristic from which estimates of  $n_j$ ,  $v_{0j}$ , and  $T$  are inferred.

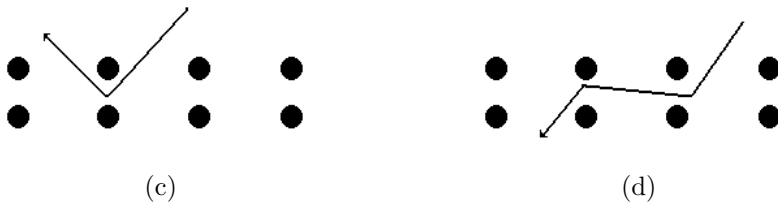


Figure 5: *Sample Ion Trajectories*

## 2.4 Need for an Improved Technique

In order to improve our analysis of RPA data, as well as future RWS data, we must characterize the effects of the grid system on the ion distributions collected. While several simulations have been carried out in recent years [2] [4], these tests do not fully characterize the effects of real grids on particle trajectories and three-dimensional distributions.

I propose to address these concerns by using the ANSYS multiphysics simulator. By using an iterative technique, ANSYS can characterize transmission coefficients for ions of specific ram energies and incidence angles. These values can then be incorporated into a new analysis technique (fully described in Chapter 3), which can be compared with Equation 2.10 to qualify and quantify changes in the fitted parameters. Based on the preliminary results from

this study, alternative grid structures may be investigated to minimize leakage and lead to more accurate measurements.

# Chapter 3

## Discrete Analysis

### 3.1 A Simple Construct

The effects of non-ideal grids can be expressed as an energy and arrival angle dependent transmission coefficient for particles encountering the grid. In order to better visualize the incorporation of these calculated transmission coefficients, we first consider a simplified case for which there is only a ram velocity associated with the incoming ions. We define a density distribution  $n$  as a function of the ram energy, or the kinetic energy due to the ram velocity ( $\frac{1}{2}mv_{\perp}^2$ ), subject to the condition

$$\mathcal{N} = \int_0^{\infty} n(\varepsilon_{\perp}) d\varepsilon_{\perp} \quad (3.1)$$

where  $\mathcal{N}$  is the density of particles moving toward the collector and  $n(\varepsilon_{\perp})$  is the density of particles as a function of ram energy. Note that  $\mathcal{N}$  is not the total density of particles, as a percentage of the particles will be moving away from the collector.

We then consider the differential flux of particles through a grid as a function of this continuous density distribution function.

$$d\psi = v_{\perp}n(\varepsilon_{\perp})d\varepsilon_{\perp} \quad (3.2)$$

where  $v_{\perp} = \sqrt{\frac{2\varepsilon_{\perp}}{m}}$ . Note that the total flux toward the collector will be

$$\Psi = \int_0^{\infty} v_{\perp}n(\varepsilon_{\perp})d\varepsilon_{\perp} \quad (3.3)$$

For collected data, we must consider discrete measurements. We will consider  $M$  values of  $\varepsilon_{\perp}$ . Thus we rewrite Equation 3.2 as

$$\Delta\psi_{(j)} = v_{\perp(j+\frac{1}{2})}n_{(j)}\Delta\varepsilon_{\perp(j)} \quad (3.4)$$

where  $\Delta\varepsilon_{\perp(j)}$  is the size of the energy bin associated with the density level of interest. Since the grid is designed to exclude particles below a given energy, we will define the energy bin as lying between the energy of interest and the next energy, *i.e.*,  $\Delta\psi_{(j)}$  is the flux of particles having ram energies between  $\varepsilon_{\perp(j)}$  and  $\varepsilon_{\perp(j+1)}$ . We must use the  $v_{\perp}$  corresponding to  $\varepsilon_{\perp(j+\frac{1}{2})}$  as the average velocity of particles in the energy bin of interest.

Now we define a vector  $\psi_j$ , of which the components are the  $M$  values of  $\Delta\psi_{(j)}$ . We define an additional vector  $I_i$ , consisting of  $N$  values, to represent the currents collected for  $N$

values of retarding voltages applied. The current vector is found to be

$$I_i = eA\tilde{T}_{ij}\psi_j \quad (3.5)$$

where  $e$  is the fundamental charge,  $A$  is the collection area, and  $\tilde{T}$  is an  $N \times M$  transformation matrix that we call the Energy Flux Index (EFI). For this and all subsequent cases, a repeated index on a given side of the equation implies a summation over that index. The function of the transformation matrix is to specify what fraction of the flux in each energy bin will pass through the RV grid under each of the  $N$  applied voltages. Note that by this definition, the transparency coefficient  $\chi$  is folded into the construction of  $\tilde{T}_{ij}$ .

If we consider only those conditions in which  $\tilde{T}_{ij}$  has an inverse, then we can solve for the flux vector.

$$\psi_j = \frac{1}{eA}\tilde{T}_{ji}^{-1}I_i \quad (3.6)$$

In this case, we restrict ourselves to  $N$  values of flux (*i.e.*,  $N = M$ ) for this solution to produce an exact value.

## 3.2 The Idealized Solution

First we look at the idealized solution of the above problem. In an ideal case, the grid itself has negligible thickness and the potential barrier it establishes is planar. There is no variation based on position or arrival angle, so either all of the flux is rejected or all of it is accepted. In this case, all components of the EFI must be either 0 or 1, scaled by the

transparency coefficient. If our set of energy values corresponds to our set of RV values, then the EFI will look like

$$\tilde{T} = \chi \begin{pmatrix} 1 & 1 & 1 & \cdots & 1 \\ 0 & 1 & 1 & \cdots & 1 \\ 0 & 0 & 1 & \cdots & 1 \\ \vdots & \vdots & \vdots & \ddots & \vdots \\ 0 & 0 & 0 & \cdots & 1 \end{pmatrix} \quad (3.7)$$

where  $\chi$  is the optical transparency of the grid stack.

Likewise, the inverse of this matrix is reduced to

$$\tilde{T}^{-1} = \frac{1}{\chi} \begin{pmatrix} 1 & -1 & 0 & \cdots & 0 \\ 0 & 1 & -1 & \cdots & 0 \\ 0 & 0 & 1 & \cdots & 0 \\ \vdots & \vdots & \vdots & \ddots & \vdots \\ 0 & 0 & 0 & \cdots & 1 \end{pmatrix} \quad (3.8)$$

Note that by applying this inverted EFI matrix to the vector  $I_i$ , we end up with

$$\Delta\psi_{(j)} = \frac{1}{e\chi A} [I_{(j)} - I_{(j+1)}] \quad (3.9)$$

which is analogous to our definition of relative fluxes described in Equation 1.1.

### 3.3 Perturbation Considerations

If we consider a realistic grid system where a small fraction of the ions near the stopping potential may leak through the grid, then the morphology of the EFI becomes slightly different. The upper triangle of the EFI will be unchanged, but the values just below the diagonal will be replaced by fractional values.

$$\tilde{T} = \begin{pmatrix} \chi & \chi & \chi & \cdots & \chi \\ f_{12} & \chi & \chi & \cdots & \chi \\ f_{22} & f_{23} & \chi & \cdots & \chi \\ \vdots & \vdots & \vdots & \ddots & \vdots \\ 0 & 0 & 0 & \cdots & \chi \end{pmatrix} \quad (3.10)$$

The bottom right corner of the lower triangle will remain unchanged, as only particles near the stopping potential will leak through the grid. Note that by definition

$$f_{ij} \leq \chi \quad (3.11)$$

The relative magnitude of the  $f_{ij}$  terms effectively quantify the leakage of the non-ideal grid geometry under consideration.

### 3.4 The General Solution

This tensor system of analysis can quickly be generalized to include angular dependence. We now define  $\psi_{jkl}$  as a 3-rank tensor which describes the flux distribution as a function of ram energy ( $j$ ) and of angles in spherical coordinates ( $k, l$ ). Again, we can characterize the transmission coefficients as a function of all of these variables plus the applied retarding potential ( $i$ ), yielding a 4-rank tensor EFI. Again, we sum over all repeated indices on the right-hand side.

$$I_i = eA\tilde{T}_{ijkl}\psi_{jkl} \quad (3.12)$$

This becomes increasingly complicated should this equation be incorporated into a least-squares fitting routine. While this equation can be used to describe any flux distribution, we will limit ourselves to one specific case for the initial study.

### 3.5 A Proposed Solution

We first assume is that there is no drift transverse to the ram direction and that the flux distribution is cylindrically symmetric about the ram velocity axis. The advantage of this setup is that the number of fit parameters is reduced. This specific case can be described by

$$I_i = eA \left[ \tilde{T}_{ij} \psi_j + \tilde{T}'_{ijk} \psi'_{jk} \right] \quad (3.13)$$

Note that the first term in the brackets is identical to the simpler case outlined in Sections 3.1-3.3. This is the part of the distribution which has no transverse velocity. The second (primed) term in brackets describes the components which approach at a small angle. For a cylindrically symmetric drifting Maxwellian distribution, we can relate  $\psi$  to  $\psi'$  by

$$\psi'_{jk} = f_k \psi_j \quad (3.14)$$

where  $f_k$  is a proportionality constant related to the distribution for the  $k^{th}$  incidence angle.

Equation 3.9 can be rewritten as

$$I_i = eA \left[ \tilde{T}_{ij} + \tilde{T}'_{ijk} f_k \right] \psi_j \quad (3.15)$$

It should be mentioned that each value of  $\tilde{T}'_{ijk}$  must be an average of the transparency coefficients over the azimuthal angle  $b$ , as shown in Figure 6. This is done to enforce cylindrical symmetry across the system.

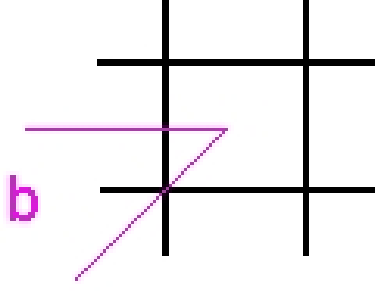


Figure 6: *Azimuthal Angle  $b$  in the Grid Plane*

The immediate benefit of the form of Equation 3.15 is that it allows us to quickly judge the effects of angular dependency. In a case where there is no angular dependence, we see that the ram EFI ( $\tilde{T}_{ij}$ ) should be proportional to the angular EFI ( $\tilde{T}'_{ijk}f_k$ ), since both will act in the same way upon the flux vector. This can be characterized by

$$\sum_k \tilde{T}'_{ijk}f_k = \zeta \tilde{T}_{ij} \quad (3.16)$$

where  $\zeta$  is constant for all  $i, j$ .

Note that all the components of the generalized EFI ( $\tilde{T}_{ijkl}$ ) still must be calculated for this process. The assumptions are made to simplify the data-fitting process. These assumptions can easily be tested, as explained in the following chapter.

## 3.6 Data Fitting

By using a least-squares fitting routine, we can construct  $f_k$  and  $\psi_j$  for a given drifting Maxwellian distribution and replace the Knudsen equation (2.10) with Equation 3.15 in standard fitting routines. As a validation of this approach, we can simulate the case in which  $\tilde{T}_{ijkl}$  takes on its ideal form and compare the results with Equation 2.10.

# Chapter 4

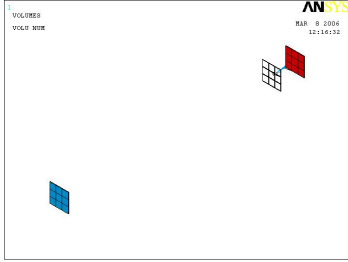
## Methodology

### 4.1 A Brief Description of ANSYS

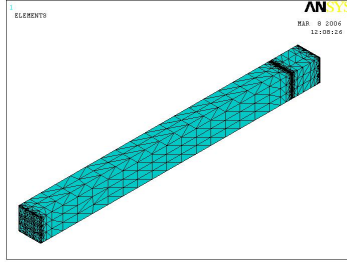
The EFI can be constructed using the ANSYS Multiphysics simulation software. ANSYS is a Finite Element Analysis (FEA) tool used for the simulation of many physical phenomena, including structural, thermal, and electromagnetic analysis.

A three-dimensional geometry is defined, such as that seen in Figure 7e. Physical properties such as relative permeability and permittivity are defined and associated with given volumes, and boundary conditions are set according to user specifications.

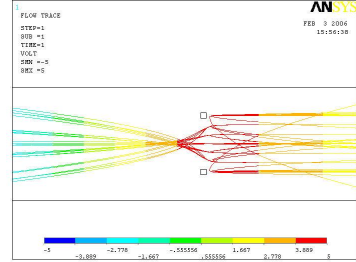
The software then defines a three-dimensional adaptive mesh over the specified geometry, as shown in Figure 7f. The shape and size of the cells is variable based on several user inputs and may be altered to optimize the calculations.



(e) Solid Elements in ANSYS



(f) All Elements Meshed



(g) Ion Trajectories

Figure 7: *Some capabilities of ANSYS. These were made using a sample construction module.*

The user can then specify voltages to apply to certain volumes. In this case, the voltages are applied to the RV grid and the front and back ends of the 3D brick in Figure 7e. The software applies these voltages to the nodes of each cell in the volumes of interest and calculates the potential at each of the remaining nodes in the free space surrounding the grids. From this, ANSYS can also calculate the electric field at each node.

Ion optics is another task easily handled by ANSYS. Once the electric field is calculated for all space in the simulation, a charged particle can be placed anywhere within the volume according to user-defined initial conditions, including charge, mass, position and initial velocity. The trajectory path can then be calculated and displayed, as shown in Figure 7g.

## 4.2 Verification

In order to verify the ANSYS method of solution, I propose to first run the simulation using an idealized grid, as described in Section 2.1. The criteria for success is that the EFI constructed by the ANSYS routine will be identical to the ideal EFI (Equation 3.7).

## 4.3 Research Approach and Goals

The research of this project can be carried out in three distinct steps.

1. Construct an RV grid system in ANSYS to build the EFI
2. Develop FORTRAN code to simulate IV curves using the EFI
3. Develop and test FORTRAN code for curve-fitting using the EFI

The overall goals of this work are:

- A. Characterize the effects of a non-ideal grid on a drifting Maxwellian distribution of particles. (achieved by completion of Step 1)
- B. Quantify the errors that grid and arrival angle effects introduce into the measurement of  $n_j$ ,  $v_{j0}$ , and  $T$  in standard curve-fitting analysis. (achieved by completion of Steps 2 and 3)
- C. Suggest improvements in grid designs and analysis techniques that will reduce these errors. (achieved by further iterations of Steps 1, 2, and 3)

### 4.3.1 The ANSYS Code

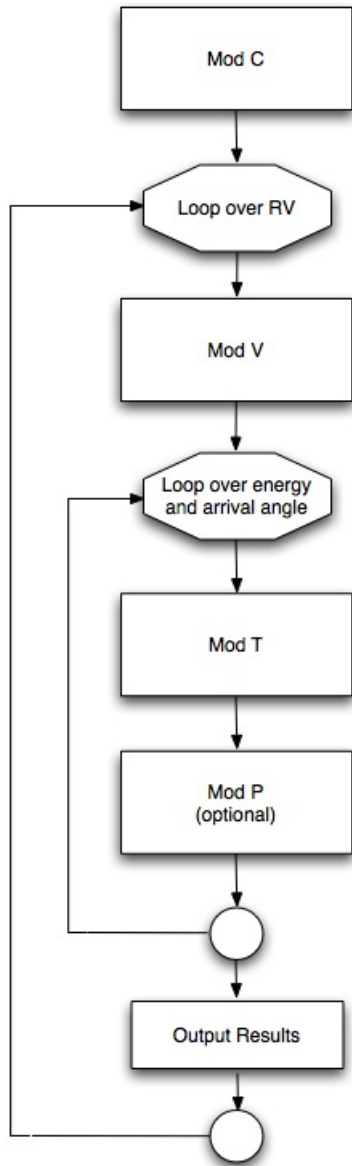
The ANSYS code in development is constructed as a modular system in order to simplify both the development process and future modifications to accommodate other grid geometries and incident particle distributions. The four modules described below can be seen in the flow chart in Figure 8.

The Construction Module (Mod C) specifies the three-dimensional geometry of the RV grid and the surrounding volume under consideration. It also applies material properties to the specified volumes, specifies boundary conditions, and defines the mesh. While a sample Module C has been constructed to test the capabilities of ANSYS, the module specific to the geometry of interest is still under construction.

The Voltage Module (Mod V) applies a specified voltage to RV grid and sets the boundary plates to ground. It then calculates the potential and electric field everywhere in the 3D volume. Module V is currently complete and has been tested for sample geometries in test versions of Module C.

The Transmission Module (Mod T) specifies the properties of individual ions, including velocity, attack angle, charge, and mass. The module then calculates a trajectory for for a single ion at a given position and repeats this process for many positions, as determined by a random number generator. This is repeated many times ( $> 10,000$ ) to simulate a large population passing through the grids, and the fraction of those ions transmitted is saved to file, along with the corresponding RV,  $\varepsilon_{\perp}$ , and angular information. Module T is currently under construction.

The Trajectory Path Module (Mod P) is an optional module that displays the ion paths as a function of position for a given ion energy / angle combination and applied RV. Module P saves these tracks to an image file for demonstration purposes. It is currently complete.



Module	Functions
C	Construct Geometry Mesh Volume
V	Apply Voltages Calculate Resultant Fields
T	Calculate Transmission Save EFI info to file
P	Display Particle Paths Save Path as JPG

Table 1: *Functions of ANSYS Modules*

Figure 8: *Flowchart for the ANSYS Modules*

### 4.3.2 The FORTRAN Simulator

The second step is to write a program to process the ANSYS output to produce a simulated IV curve for a given Maxwellian distribution. This code will utilize the EFI generated by the ANSYS code and the general equation described previously (Equation 3.12). The Maxwellian distribution for a given set of input parameters ( $n_{0j}$ ,  $v_{0j}$ ,  $\alpha$ ,  $b$ ,  $T$ ) can be calculated for all components of the tensor  $\psi_{jkl}$ . Random noise of a specified level may be added to better simulate real collected data. In addition, the curve can be decimated to simulate data collection with sample and hold Analog-to-Digital (ADC) Circuit.

### 4.3.3 The Data-Fit Routine

The third step is broken into two parts. The first is to fit this simulated IV curve with a traditional fit routine; the second is to fit the curve with the new technique outlined in Section 3.5. Errors on the fitted parameters can then be quantified for several sets of input parameters for both codes.

The validity of neglecting the cross-track velocity in the fit can also be determined during this stage. Additional simulations can be generated for several cross-track drift velocity inputs, and the errors on the fit parameters can be quantified by repeating Step 3 for these cases.

# Chapter 5

## Summary and Conclusions

The program of study outlined in this proposal will extend the current state of knowledge by considering several shortcomings of retarding grid-type devices to a level not previously studied. By using the discrete analysis approach outlined in Chapter 3, we will obtain both a numerical analysis tool and a convenient method for visualizing the relative flux leakage of non-ideal grids. This method allows for ease in comparison of the effectiveness of different grid geometries. By incorporating the ANSYS simulation tool into our analysis, we will be able to realistically quantify the effects of the grid on both the IV characteristics and the fit parameters inferred from them. All of these approaches will be new areas of applied research, and should therefore be publishable in journals such as *Reviews of Scientific Instruments* or *IEEE Transactions on Plasma Science*. We anticipate at least two such publications: one covering the effects of various grid geometries on the EFI, and a second quantifying the changes in inferred parameters caused by neglecting the effects of non-ideal grids.

The approximate time frame for completion of this work is given in the table below.

Milestone	Estimated Completion
Complete ANSYS Modules	Fall 2006
Complete Code Validation	Fall 2006
Compare EFI for Ideal and non-Ideal cases	Spring 2007
Publish Results	Summer 2007
Complete FORTRAN Analysis Codes	Fall 2007
Perform IV case studies to quantify effects on inferred parameters	Fall 2007
Publish Results	Spring 2008
Defend Thesis	Summer 2008

Table 2: *Estimated Time Frame for Completion*

# Bibliography

- [1] Brown, Richard J.C., Paul J. Brewer and Martin J.T. Milton, The physical and chemical properties of electroless nickel-phosphorous alloys and low reflectance nickel-phosphorous black surfaces, *J. Mater. Chem.*, **12**, 2749-2754, 2002
- [2] Chao, C.K., S.-Y. Su, H.C. Yeh, Grid effects on the derived ion temperature and ram velocity from the simulated results of the retarding potential analyzer data, *Adv. Space Res.*, **32**, 2361, 2003
- [3] Chao, C.K., S.-Y. Su, H.C. Yeh, Ion temperature crests and troughs in the morning sector of the low-latitude and midlatitude topside ionosphere, *J. Geophys. Res.*, **109**, A11303, 2004
- [4] Enloe, C.L., and J.R. Shell, Optimizing the energy resolution of planar retarding potential analyzers, *Rev. Sci. Instrum.*, **63**, 1788, 1992
- [5] Hanson, W.B., D.R. Frame, J.E. Midgely, Errors in retarding potential analyzers caused by nonuniformity of the grid-plane potential, *J. Geophys. Res.*, **77**, 1914, 1972
- [6] Hanson, W.B., D.R. Zuccaro, C.R. Lippincott, and S. Sanatani, The retarding potential analyzer on atmospheric explorer, *Radio Sci.*, **8**, 333, 1973

- [7] Hanson, W.B., R.A. Heelis, R.A. Power, C.R. Lippincott, D.R. Zuccaro, B.J. Holt, L.H. Harmon, and S. Sanatani, The Retarding Potential Analyzer for Dynamics Explorer B, *Space Sci. Inst.*, **5**, 503, 1981
- [8] Hanson, W.B., and R.A. Heelis, A satellite anemometer, Final Report for NASA Grant NAGW-2534, 1993
- [9] Hanson, W.B., U. Ponzi, C. Arduini, and M. DiRuscio, A satellite anemometer, *J. Astro. Sciences*, **40**, 429, 1993
- [10] Knudsen, W.C., Evaluation and demonstration of the use of retarding potential analyzers for measuring several ionospheric quantities, *J. Geophys. Res.*, **71**, 4669, 1966
- [11] Whipple, E.C., The Ion-Trap Results in "Exploration of the Upper Atmosphere with the Help of the Third Soviet Sputnik", *Proc. IRE*, **47**, 2023, 1959